

# Ultrastructure Morphological Characterization of Different Passages of Rat Dental Follicle Stem Cells at *In vitro* Culture

Fakhri A. Al-Bagdadi, Humberto M. Barona<sup>1</sup>, Eduardo Martinez-Ceballos<sup>2</sup>, Shaomian Yao

Department of Comparative Biomedical Sciences, School of Veterinary Medicine, Louisiana State University, Departments of <sup>1</sup>Mathematics and <sup>2</sup>Biology, Southern University and A and M College, Baton Rouge, LA, USA

## Abstract

**Introduction:** Stem cells play important roles in tissue renewal and repair. Tissue-derived stem cells have been demonstrated for their applications in tissue engineering and regenerative medicine. Expansion of primary stem cells isolated from tissues to a large quantity through *in vitro* culture is needed for application of the stem cells. However, it is known that tissue stem cells commonly reduce or lose their stemness properties during *in vitro* culture. In this study, we assessed ultrastructural changes of rat dental follicle stem cells (DFSCs) during *in vitro* culture. It is our attempt to explain the loss of stemness properties in cultured tissue-stem cells at the ultrastructural level. **Method:** DFSCs was isolated from first molars of Sprague Dawley rat pups and cultured in medium consisting of alpha-MEM plus 20% FBS. Cells were passaged at 1 to 3 ratio at 90% confluence, and collected at passages 3, 6, 7 and 9 for assessment of ultrastructure morphology by transmission electron microscopy. **Results:** Of the four passages (3, 6, 7, and 9) examined, dilated rough endoplasmic reticulum (RER) was abundant in Passage 3 but less so in Passages 6, 7, and 9. The dilated RER contained lipid in Passages 3, 7, and 9. The mono- and polyribosomes in Passages 3 and 6 were located between the mitochondria and the RER. Mono- and polyribosomes were abundant in Passage 7, although mainly monoribosomes were present in Passage 9. Membrane-bound glycogen granules were in vacuoles bulging off the cells in Passage 3. Some glycogen granules were grouped in the periphery of a stem cell in Passage 9. Nuclei shapes were irregular and mainly euchromatic in Passages 6, 7, and 9. The mitochondria were dark and scarce in Passage 9; irregular, small, and dark in Passage 7; and small and rounded in Passage 6, and they were spread in the cytoplasm away from the nucleus in Passage 3. Cell contacts were seen in Passages 6, 7, and 9. The ultrastructure morphology of the examined DFSCs was not very different from the morphology criteria of the undifferentiated cells. Large vacuoles in Passage 3 were mainly at the periphery of the cell, with the small vacuoles in the cell center. Small vacuoles were scattered in the cell center of Passage 6 and the larger ones were observed at the cell's periphery. **Conclusions:** We observed the following ultrastructural changes: decreases of fine cell cytoplasmic processes, dilated cytoplasmic vacuoles, cytoplasmic pinocytotic vesicles, and nuclear heterochromatin with increasing cell passage number. Conversely, mean ratios of lipid globules, nuclear euchromatin, irregular nuclear shape, and cell contact between cells were increased with passage number. The observations may suggest an increase in committed cells among the population after long-term culture of DFSCs.

**Keywords:** Dental follicle, mitochondria, nuclei, stem cells, transmission electron microscopy, ultrastructure

## INTRODUCTION

Stem cells play a pivotal role in the development of tissues and organs, as well as maintaining homeostasis and integrity of multicellular organisms.<sup>[1]</sup> According to Varga *et al.*,<sup>[2]</sup> human dental pulp-derived stem cells are capable of differentiating into osteoblasts, odontoblasts, adipocytes, and neuronal-like cells with the potential to be used in tissue regeneration.<sup>[3-6]</sup> As an example, Zheng *et al.*<sup>[7]</sup> applied stem cells from deciduous tooth to help the regeneration of bone in mandibular defects in an animal model. It has been indicated by Karaoz *et al.*<sup>[8]</sup> that stem cells can differentiate into osteoblasts<sup>[9]</sup> or muscle

cells<sup>[10]</sup> in response to specific stimuli. It is anticipated that future research will be focusing on the use of stem cells on cell therapy, drug discovery, and tissue engineering.<sup>[11]</sup>

Exploring information about stem cells on all levels has attracted the attention of both scientists and the public

**Address for correspondence:** Dr. Fakhri A. Al-Bagdadi,  
Department of Comparative Biomedical Sciences, School of Veterinary  
Medicine, Louisiana State University, Baton Rouge, LA 70803, USA.  
E-mail: falbag1@lsu.edu

This is an open access journal, and articles are distributed under the terms of the Creative Commons Attribution-NonCommercial-ShareAlike 4.0 License, which allows others to remix, tweak, and build upon the work non-commercially, as long as appropriate credit is given and the new creations are licensed under the identical terms.

**For reprints contact:** reprints@medknow.com

**How to cite this article:** Al-Bagdadi FA, Barona HM, Martinez-Ceballos E, Yao S. Ultrastructure morphological characterization of different passages of rat dental follicle stem cells at *In vitro* culture. J Microsc Ultrastruct 2019;7:57-64.

### Access this article online

#### Quick Response Code:



**Website:**  
<http://www.jmau.org/>

**DOI:**  
10.4103/JMAU.JMAU\_44\_18

alike because this research provides the promise of tissue regeneration, drug screening, cell therapy, disease modeling, and organogenesis.<sup>[12]</sup> Furthermore, pluripotent stem cells hold significant promise for the treatment of tissue deficiencies and other human diseases.<sup>[13,14]</sup> Stem cells have been applied in acute injuries and myocardial infarctions.<sup>[15]</sup> Adult stem cells represent a practical research model for regenerative medicine, correction of genetic disorders,<sup>[16]</sup> and tissue engineering.<sup>[17]</sup>

According to Pasquinelli *et al.*,<sup>[18]</sup> a detailed ultrastructural morphological identity of adult stem cells and their differentiating abilities is limited. Light microscopy resolution limitations do not provide efficient analysis of stem cell differentiation into functional tissues, which is a major challenge in stem cell research.<sup>[11]</sup> Various parameters should be applied to characterize stem cells through ultrastructure morphology<sup>[8]</sup> since this technique allows for the visualization of normal cell traits and anomalies.<sup>[19]</sup> Transmission electron microscopy provides ultrastructure of unsurpassed details of the cell's subcellular organelle organization.<sup>[20]</sup> Baharvand and Matthaei<sup>[21]</sup> indicated that the ultrastructure of human<sup>[22]</sup> and nonhuman primate<sup>[23]</sup> embryonic stem (ES) cells and pig ES-like cells<sup>[24]</sup> has been reported. The ultrastructure of mouse ES cells was also reported by Desbaillets *et al.*<sup>[25]</sup> Furthermore, the ultrastructure of human ES cells has been examined at Passage 35 by Sathananthan *et al.*<sup>[22]</sup>

Efficient stem cell differentiation into specific functional tissue is an important question.<sup>[11]</sup> Adult stem cells lose differentiation abilities during *in vitro* culture at late passages.<sup>[26-28]</sup> Li *et al.*<sup>[29]</sup> studied human mesenchymal stem cells in Passages 10, 11, 13, 21, and 40. Stem cells at various passages have been examined by interested researchers such as Sathananthan *et al.*<sup>[22]</sup> at Passage 35; Park *et al.*<sup>[30]</sup>: over 40 passages; Karaoz *et al.*<sup>[8]</sup>: passage 3 through Passage 25; Li *et al.*<sup>[29]</sup>: passage 10; Høffding and Hyttel<sup>[31]</sup>: passage 53; and Csaki *et al.*<sup>[32]</sup>: passages 3 and 4. However, no comprehensive analysis has been taken to characterize the ultrastructure of adult stem cells in various passages. Furthermore, the ultrastructural characteristics of dental follicle stem cells (DFSCs) are not available in the current literature. In this current study, we attempted to examine the ultrastructure morphology of DFSCs of different passages. Our work provides valuable information regarding stem cells that are easily accessible from tissue resources and that hold promise as a therapeutic approach for tissue reconstruction.<sup>[33]</sup> The fine structure morphology of stem cells at various passages can help to understand the function of these cells based on the contents and integrity of their subcellular organelles.

Stem cells play an important role in the development of tissues and organs as they maintain the homeostasis and integrity of multi-celled organisms.<sup>[2]</sup> Because the capacity of cultured human dental stem cells to differentiate into odontoblasts<sup>[2]</sup> may be affected by the passage number, the aim of this study is to characterize the ultrastructure morphology of rat dental follicle-derived stem cells (DFSCs) in different Passages. To achieve the aim, we used electron microscopy and statistical analyses to define the ultrastructural features of rat DFSCs at

multiple passages: 3, 6, 7, and 9. Based on our statistical analysis, we observed that mean ratios for ultrastructure characteristics such as fine cell cytoplasmic processes, dilated cytoplasmic vacuoles, cytoplasmic pinocytotic vesicles, and nuclear heterochromatin, decreased with increasing passage number. Conversely, mean ratios for ultrastructural characteristics such as lipid globules, nuclear euchromatin, Irregular nuclear shape, and cell contact between cells, increased with passage number. As an increase in cell-cell contact and in the number of lipid globules may indicate an increase in committed cells towards an adipogenic lineage among the population of cultured DFSCs. Our findings suggest that DFSCs cultured for seven or more passages show evidence of loss of stemness during *in vitro* expansion. Thus, our results may shed light on the understanding, at the ultrastructural level, of loss of differentiation potential seen during the *in vitro* culture of dental follicle stem cells.

## MATERIALS AND METHODS

### Tissue culture

Sprague Dawley rats were housed at the Louisiana State University's School of Veterinary Medicine for breeding postnatal pups. Dental follicles were isolated from first mandibular molars of rat pulps at postnatal day 6 or 7. Tissues were then sliced into small pieces and digested with trypsin to obtain the cell suspension. For DFSC cultures, cells were cultured in alpha-minimum essential medium supplemented with 20% fetal bovine serum and incubated at 37°C and 5% CO<sub>2</sub>. Cultures established in this medium contain stem cells (i.e., DFSCs) that are capable of differentiation. When cells reached 90% confluence, they were passaged to fresh flasks at a 1–3 ratio (i.e., 1 flask passaged to 3 flasks) until the desired passages. The stem cells of each passage were individually pelleted in 1.5- $\mu$ l Eppendorf tubes by centrifugation at 4000 RPM in an Eppendorf 5415 centrifuge (Brinkman Instruments Inc., Cantiague Road, Westbury, NY 11590, USA). Pellets were washed in PBS and fixed in a mixture of 2% paraformaldehyde and 1.25% glutaraldehyde in 0.1M cacodylate (NaCac) buffer supplemented with 5% sucrose for 2 h. The pellets were removed from the tubes, embedded in 3% agarose, cut in milliliter cubes, washed several times in the same buffer, and postfixed in 1% osmium tetroxide for 1 h.

### Ethanol treatment and sample preparation

After washing in water, samples were incubated with 2% uranyl acetate in sodium acetate buffer (pH = 3,5) for 2 h, washed in water, dehydrated in ascending ethanol series and propylene oxide, and embedded in Epon-Araldite. Blocks were sectioned with Ultramicrotome (Leica EM UC7). Three thin 70–80-nm sections were made from each capsule by skipping one-micron thick section between each of the examined section to avoid the already examined cells.

### Transmission electron microscopy

The sections were stained with lead citrate and examined in a JEOL JEM-1011 microscope with an attached HAMAMATSU ORCA-high-resolution digital camera. All

reagents and supplies for electron microscopy were from EMS (Fort Washington, PA, USA). Each of the examined sections of each passage was studied, and labeled digital pictures were taken from each examined grid and saved on a USB for further analysis and investigation. The mitochondria of the complete stem cell pictures were counted and recorded.

**Data analysis**

For each of the 12 variables examined (fine cell processes, dilated RER profiles, mitochondria density, dilated cytoplasmic vacuoles, lipid globules, cytoplasmic pinocytotic vesicles, Golgi, nuclear heterochromatin, nuclear euchromatin, regular nucleus shape, irregular cell shape, and contact between cells), the mean in each passage ( $\mu_3, \mu_6, \mu_7,$  and  $\mu_9$ ) was calculated by dividing the variable count obtained in each passage by the total number of cell examined from that passage. Considering

Passage 3 as the control passage, we divided all sample means by Passage 3 mean to obtain the relative mean ratios (i.e., with respect to the mean of Passage 3),  $\hat{\mu}_3, \hat{\mu}_6, \hat{\mu}_7,$  and  $\hat{\mu}_9$ . The collected data included the values of the count, the mean  $\mu_i$  and relative mean  $\hat{\mu}_i$  for passages  $i = 3, 6, 7,$  and  $9$  in all the 12 variables within the ultrastructure morphology matrix. To test the differences between the means in each of the 13 variables of stem cells from rat dental sacs at Passages 3, 6, 7, and 9, the following hypotheses were considered:

$$H_0: \hat{\mu}_3 = \hat{\mu}_6 = \hat{\mu}_7 = \hat{\mu}_9$$

$$H_1: \hat{\mu}_3 \neq \hat{\mu}_6, \hat{\mu}_3 \neq \hat{\mu}_7, \hat{\mu}_3 \neq \hat{\mu}_9$$

Where  $\hat{\mu}_3, \hat{\mu}_6, \hat{\mu}_7,$  and  $\hat{\mu}_9$  are the ratios of the sample mean of Passages 3, 6, 7, and 9, respectively, with respect to the mean of

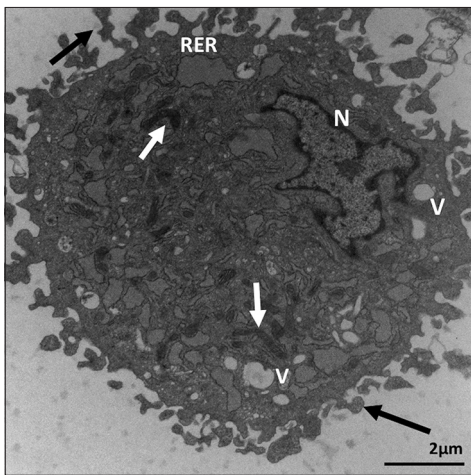


**Figure 1:** Ultrastructure of Passage 3 dental follicle stem cells. It shows dilated rough endoplasmic reticulum, vacuoles (V), elongated mitochondria (white arrows), and abundant coarse microvilli (black arrows). N = Irregular nucleus with marginated heterochromatin. X 12,000. Scale bar: 2 μm

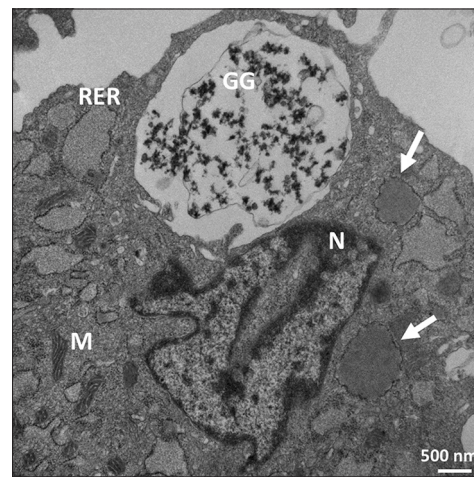


**Figure 2:** Ultrastructure of Passage 3 dental follicle stem cells. It shows dilated rough endoplasmic reticulum; some contain lipid (arrows). Scattered mitochondria of various shapes with distinct cristae (M) are also observed. X 24,900. Scale bar: 500 nm. 80 KV

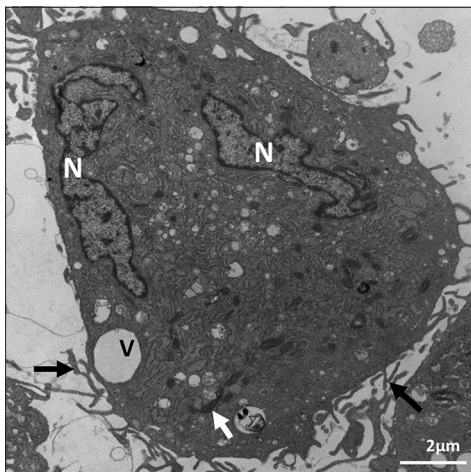


**Figure 3:** Ultrastructure of Passage 3 dental follicle stem cells. It shows abundant rough endoplasmic reticulum, elongated mitochondria (arrow), cellular microvilli (arrows), and two irregular euchromatic nuclei (N) with narrow rims of heterochromatin. It is a cementoblast. X 1000

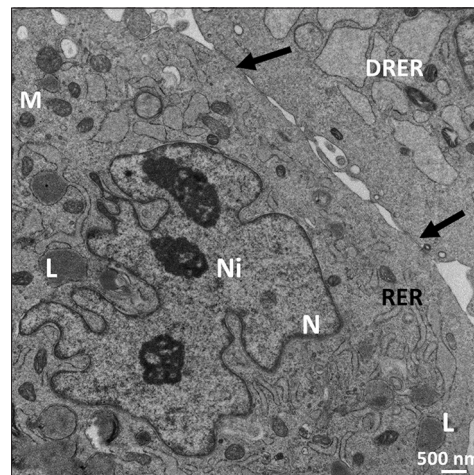


**Figure 4:** Ultrastructure of Passage 7 dental follicle stem cells. It shows dilated rough endoplasmic reticulum, mitochondria (M), irregular euchromatic nucleus (N), nucleoli (Ni), and dilated rough endoplasmic reticulum with lipid droplets (L). Cell junctions (arrows) are observed. X 19,200. Scale bar: 500 nm. 80 KV

**Table 1: Summary statistics for the effect of cell passage number on mouse dental follicle stem cells**

Variables	$P_3$ (44 cells)			$P_6$ (35 cells)			$P_7$ (21 cells)			$P_9$ (37 cells)		
	Count	$\mu_3$	$\hat{\mu}_3$	Count	$\mu_6$	$\hat{\mu}_6$	Count	$\mu_7$	$\hat{\mu}_7$	Count	$\mu_9$	$\hat{\mu}_9$
Fine cell process	51	1.16	1	32	0.91	0.78879	7	0.33	0.28758	20	0.54	0.46634
Dilated cytoplasmic vacuoles	76	1.73	1	54	1.54	0.89323	20	0.95	0.55137	29	0.78	0.45377
Cytoplasmic pinocytotic vesicles	84	1.91	1	40	1.14	0.59863	23	1.10	0.57369	32	0.86	0.45302
Nuclear heterochromatin	44	1.00	1	26	0.74	0.74285	11	0.52	0.52381	17	0.46	0.45945
Lipid globules	20	0.45	1	0	0.00	0.00000	27	1.29	2.82857	58	1.57	3.44864
Nuclear euchromatin	135	3.07	1.0	106	3.03	0.98709	69	3.29	1.07089	136	3.68	1.19799
Regular nuclear shape	2	0.05	1.0	5	0.14	3.14285	9	0.43	9.42857	16	0.43	9.51351
Contact between cells	0	0.00	0.0	0	0.00	0.00000	46	2.19	1.00000	124	3.35	1.52996
Dilated RER profiles	142	3.23	1	69	1.97	0.61086	36	1.71	0.53118	101	2.73	0.84583
Irregular cell shape	67	1.52	1	35	1.00	0.65671	29	1.38	0.90689	54	1.46	0.95845
Mitochondria density	100	2.27	1	89	2.54	1.11885	31	1.48	0.64952	58	1.57	0.68973
Golgi apparatus	2	0.05	1	0	0.00	0.00000	0	0.00	0.00000	0	0.00	0.00000

Relative mean ratios ( $\hat{\mu}$ ) were calculated with respect to Passage 3 (control). RER: Rough endoplasmic reticulum

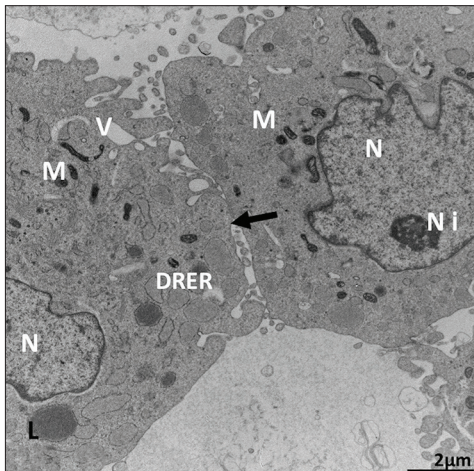


**Figure 5:** Ultrastructure of Passage 9 dental follicle stem cells. It shows contact between cells (arrow) and nuclei (N) containing mainly euchromatin. Scattered vacuoles (V), several lipid globules (L), and mitochondria (M) are observed. X 10,000. Scale bar: 2  $\mu$ m. 80 KV

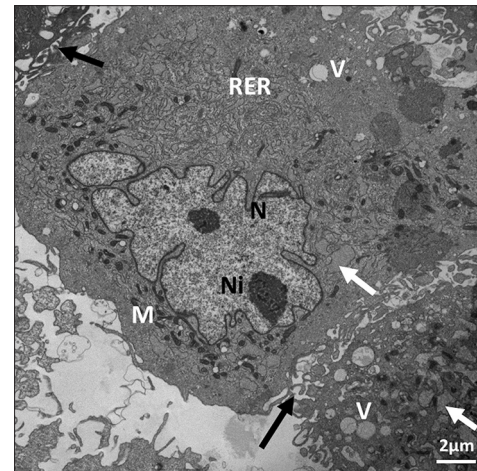


**Figure 6:** Ultrastructure of Passage 6 dental follicle stem cells. It shows dilated rough endoplasmic reticulum (arrows), electron-dense mitochondria (M), irregular euchromatic nucleus (N) with two nucleoli (Ni), scattered vacuoles (V), and neighboring stem cell (black arrows). X 19,200. Scale bar: 2  $\mu$ m. 80 KV

the control Passage 3. Based on the results obtained, histograms were created with MATLAB 2017b and EXCEL 2010.

## RESULTS

### Ultrastructural morphology

We observed ultrastructural changes at different Passages of 3, 6, 7, and 9. The ultrastructure of the stem cells in all passages showed mainly irregular euchromatin nuclei [Figures 1-5] with narrow irregular margined heterochromatin. The ultrastructure of the examined Passages 3, 6, 7, and 9 showed eccentric irregular nuclei in all the passages, and some nuclei were central in Passages 6, 7, and 9 [Figures 4-6]. Narrow rim of heterochromatin was present in the nuclei of Passages 3 and 6 [Figures 1-3 and 6]. The inner zone in all the passages contained all the subcellular organelles, and Passages 7 and 9 indicated that part of the peripheral cellular zone of some cells lacked subcellular organelles and contained various vacuoles or coated pits. The rough endoplasmic reticulum (RER) was

dilated and contained granular material in all the passages. It also contained lipid-like material in all the passages except Passage 3. Lipid-like material was abundant in Passage 9 [Figure 5]. Well-developed Golgi apparatus in Passage 3 but none was seen in Passages 6–9 [Table 1]. With regard to the mitochondria, they were elongated, dark colored, and spread on one side of the nucleus at Passage 3 [Figure 1]. At Passage 6, they were elongated, dark colored, and spread around the nucleus and some were around the nucleus [Figure 6]. At Passage 7 [Figure 4], they were elongated, irregular, and dark stained. At Passage 9 [Figure 5], mitochondria were small, dark, and were found in less amount around the nucleus. Regarding to vacuoles, at Passage 3, a large vacuole was located at the periphery and a small one was in the center [Figures 1 and 3]. Passage 6 vacuoles were small and abundant in the periphery; large ones were irregular and contained multiple vesicles [Figure 6]. Passage 7 vacuoles were of various shapes, less in number, and some were budding [Figure 4]. In Passage 9,

very few small vacuoles were observed [Figure 5]. Some cells were lack of vacuoles at this passage. With regard to poly- and monoribosomes, in Passages 3 and 6, they were located between the mitochondria and the RER [Figures 1-3 and 6]. Mono- and polyribosomes were observed all over the cytosol in Passage 7 and mainly monoribosomes were observed in Passage 9. Membrane-bound glycogen granules of various shapes were seen in a vacuole bulging off the cell in Passage 3 [Figure 2]. Some glycogen granules were observed grouped in the periphery of the cell in Passage 9 [Figure 5]. Lipid-like content was seen in Passage 3, and several lipid color granules were located by the nucleus in Passage 6 [Figure 6]. Some of the cells in Passage 7 showed dark lipid-like substance in the RER in various cells in the vicinity of the nucleus [Figure 4].

Abundant lipid-like dark materials were found in dilated RER in Passage 9 [Figure 5].

### Statistical analysis

The initial data obtained by transmission electron microscopy included 44 cells in Passage 3, 35 cells in Passage 6, 21 cells in Passage 7, and 37 cells in Passage 9 [Table 1]. In general, in all variables, the mean ratio showed a significant difference in the Passages 6, 7, and 9 with respect to the mean of the control Passage 3. For some of the variables [Figure 7], the mean ratio decreased consistently in all passages (fine cell processes ~20%–71%, dilated cytoplasmic vacuoles %, cytoplasmic pinocytotic vesicles, and nuclear heterochromatin 26%–54%); for others, the mean ratio generally increased with passage number (lipid globules ~ 180%–240%, nuclear

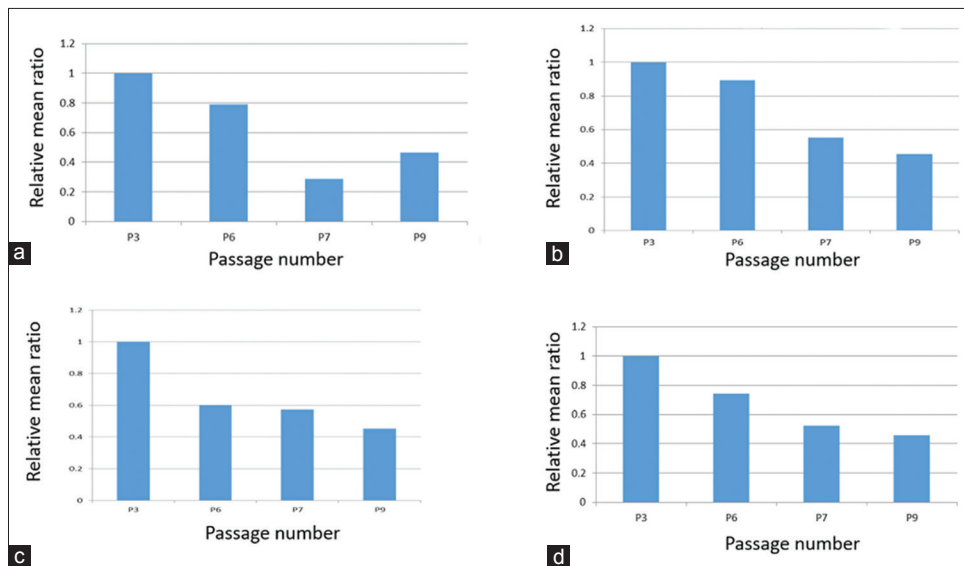


**Figure 7:** Ultrastructural cell characteristics whose mean ratios decreased with passage number. (a) Fine cell cytoplasmic processes. (b) Dilated cytoplasmic vacuoles. Decreased 16% for Passage 6, 45% for Passage 7, and 55% in Passage 9. (c) Cytoplasmic pinocytotic vesicles. (d) Nuclear heterochromatin

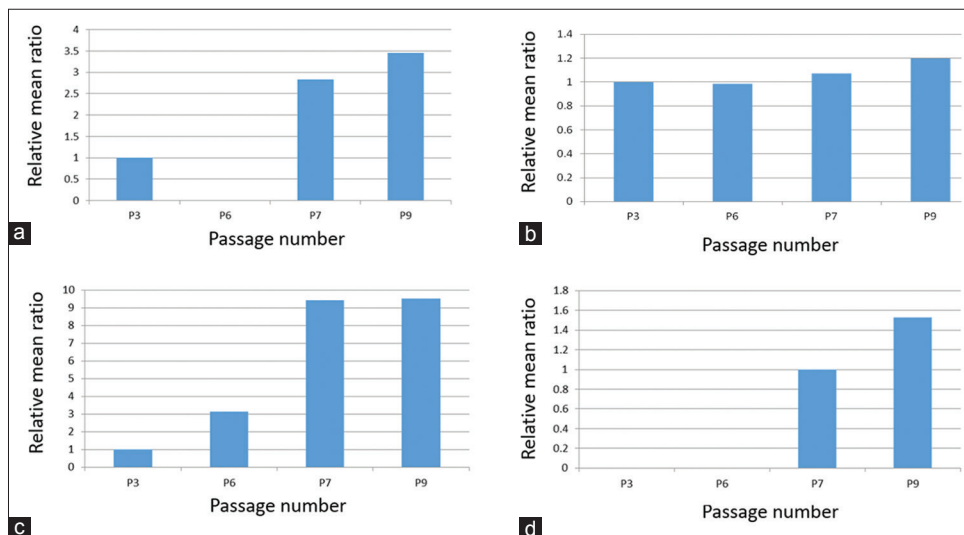


**Figure 8:** Ultrastructural cell characteristics whose mean ratios increased with passage number. (a) Lipid globules. Increases were observed in Passages 7 and 9. (b) Nuclear euchromatin. (c) Regular nuclear shape. (d) Cell contact between cells

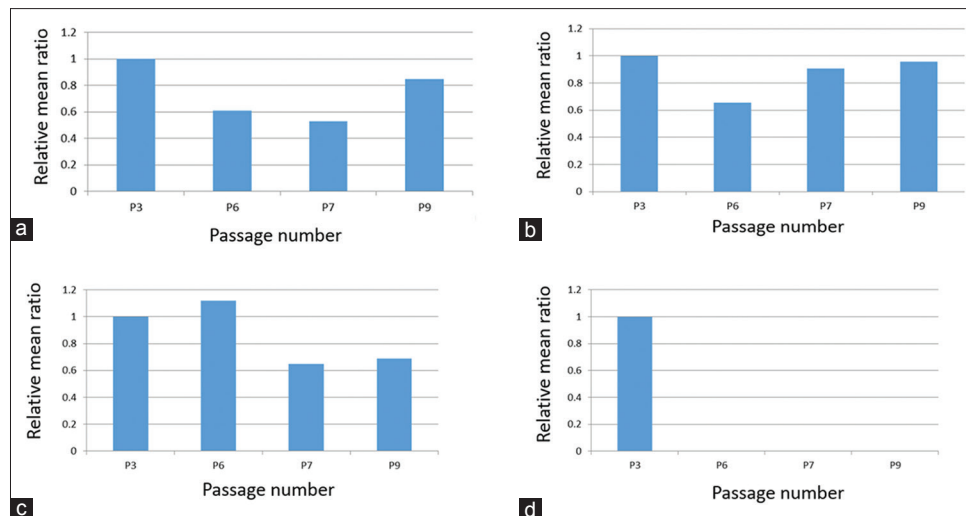


**Figure 9:** Ultrastructure characteristics with irregular pattern. (a) Dilated rough endoplasmic reticulum profiles. (b) Irregular cell shape. (c) Mitochondrial density. (d) Golgi apparatus. Only observed in Passage 3 cells

euchromatin 19%, regular nuclear shape, and contact between cells 100% and 150%) [Figure 8]. In the remaining variables [Figure 9], the mean ratio showed an irregular behavior: for dilated RER profiles and irregular cell shape, the mean ratio first decreased at Passage 6 and then increased in Passages 7 and 9 [Figure 9a and b]; for the variable mitochondria density, the mean ratio increased in Passage 6 and then decreased in Passages 7 and 9 [Figure 9c]. Finally, Golgi apparatus was observed in cells from Passage 3 but not at other passages [Figure 9d].

## DISCUSSION

Although the ultrastructure of prenatal mouse and human stem cells has been extensively examined in the literature,<sup>[18,21,34-37]</sup> most of these studies did not examine the changes of ultrastructure in different passages of the examined stem cells. For instance, Singh *et al.*<sup>[37]</sup> conducted research of human ES cells using early-to-late passages: using five serial passages to indicate that cell survival was dependent on human stem cell re-aggregation without defining the criteria of each passage in their study. However, the present study is the first to define the ultrastructural features of rat adult DFSCs in multiple passages (3, 6, 7, and 9). These criteria are comparable to those used to characterize stem cell passages of mouse postnatal dental sac: microvilli, lipid droplets, mitochondria, lysosomes, Golgi complex, dilated and nondilated rough ER, ribosomes, coated pits, vacuoles, vesicles, nucleoli, and nuclei. The abundance of long fine villi and filopodia on the surface of rat stem cells in Passages 3, 6, and 9 has also been observed on Passage 35 of human ES cells<sup>[22]</sup> and nonhuman primates.<sup>[22]</sup> They were also observed on blastocysts of mouse,<sup>[34,36,38,39]</sup> rhesus monkey,<sup>[40]</sup> rabbit,<sup>[41]</sup> baboon,<sup>[42]</sup> human,<sup>[35,43]</sup> and human bone marrow stem cells.<sup>[18]</sup>

However, long and abundant villi extensions that were present on the rat stem cells in Passages 3, 6, and 7 were not reported in other mammalian stem cells. Numerous villi, filopodia, and

pinocytotic vesicles along areas of the peripheral cytoplasm and plasma membranes of the rat stem cell dental follicle cells are presumed to increase protein absorption.<sup>[43,44]</sup> The rat DFSCs showed abundant surface blebs in Passages 6 and 9 similar to those reported in human bone marrow stem cells.<sup>[18]</sup> It is possible that the abundant surface blebs function to increase the surface area for metabolism and absorption according to Csaki *et al.*<sup>[32]</sup>

On the other hand, prominent Golgi complexes and rough ER in Passage 3 are speculated to increase protein synthesis and secretions. This feature also relates to the abundant filopodia and fine villi and pinocytotic vesicles of the rat stem cells. In this study, we observed that Passage 3 Golgi apparatus, mitochondria, and other organelles of cells were located around the vicinity of the nucleus. Some of the rat stem cells had few fine villi, which were suggested to indicate that these cells were prepared for cell division, although we have no morphological evidence. The electron-dense plaques noticed were presumed to be desmosome-like junctions. Desmosome-like cell junctions observed in our rat stem cells in Passages 6, 7, and 9 have also been widely reported in human ES cells and blastocysts of different mammals: rabbit,<sup>[45]</sup> baboon,<sup>[42]</sup> sheep,<sup>[41]</sup> bovine,<sup>[46,47]</sup> and human.<sup>[22,44]</sup> These structures are thought to function in cell-cell communication. Lipid droplets were reported in Passages 7 and 9 in this study, as well as most of the lipid globules found in dilated RER in Passages 7 and 9 of the rat stem cells, similar to those reported in the mouse.<sup>[35]</sup> Lipid droplets have been reported in pig ES-like cells<sup>[24]</sup> but were not seen in human ES cells.<sup>[22]</sup> Mitochondria in rat stem cells were elongated round to oval, electron dense, and had transverse sausage-like cristae.

## CONCLUSION

In the present study, we used electron microscopy and statistical analyses to define the ultrastructural features of rat adult DFSCs at multiple passages: 3, 6, 7, and 9. Based

on our statistical analysis, we observed that mean ratios for ultrastructure characteristics such as fine cell cytoplasmic processes, dilated cytoplasmic vacuoles, cytoplasmic pinocytotic vesicles, and nuclear heterochromatin, decreased with increasing passage number. Conversely, mean ratios for ultrastructural characteristics such as lipid globules, nuclear euchromatin, Irregular nuclear shape, and cell contact between cells, increased with passage number. As the observed increase in cell-cell contact and in the number of lipid globules may indicate an increase in committed cells towards an adipogenic lineage, our findings suggest that DFSCs cultured for seven or more passages show evidence of loss of stemness during *in vitro* expansion of dental follicle stem cells. Thus, our results may shed light on the understanding, at the ultrastructural level, of loss of differentiation potential seen during the *in vitro* culture of dental follicle stem cells.

### Acknowledgments

The authors want to thank Dr. Xiaochu Wu and Dr. Julia Sokolova for sample preparation for electromicroscopic study.

### Financial support and sponsorship

This study was financially supported by CORP grant, School of Veterinary Medicine, Louisiana State University, Baton Rouge, Louisiana, USA.

### Conflicts of interest

There are no conflicts of interest.

### REFERENCES

- Shanti RM, Li WJ, Nesti LJ, Wang X, Tuan RS. Adult mesenchymal stem cells: Biological properties, characteristics, and applications in maxillofacial surgery. *J Oral Maxillofac Surg* 2007;65:1640-7.
- Varga V, Hollý D, Vojtaššák J, Bohmer D, Polák S, Danišovič L. Morphological characterization of *in vitro* expanded human dental pulp-derived stem cells. *Biol Sect Zool* 2011;66:706-11.
- d'Aquino R, Graziano A, Sampaolesi M, Laino G, Pirozzi G, De Rosa A, *et al.* Human postnatal dental pulp cells co-differentiate into osteoblasts and endotheliocytes: A pivotal synergy leading to adult bone tissue formation. *Cell Death Differ* 2007;14:1162-71.
- Kadar K, Kiraly M, Porcsalmy B, Molnar B, Racz GZ, Blazsek J, *et al.* Differentiation potential of stem cells from human dental origin – Promise for tissue engineering. *J Physiol Pharmacol* 2009;60 Suppl 7:167-75.
- Suchanek J, Soukup T, Visek B, Ivancakova R, Kucerova L, Mokry J, *et al.* Dental pulp stem cells and their characterization. *Biomed Pap Med Fac Univ Palacky Olomouc Czech Repub* 2009;153:31-5.
- Muthna D, Soukup T, Vavrova J, Mokry J, Cmielova J, Visek B, *et al.* Irradiation of adult human dental pulp stem cells provokes activation of p53, cell cycle arrest, and senescence but not apoptosis. *Stem Cells Dev* 2010;19:1855-62.
- Zheng Y, Liu Y, Zhang CM, Zhang HY, Li WH, Shi S, *et al.* Stem cells from deciduous tooth repair mandibular defect in swine. *J Dent Res* 2009;88:249-54.
- Karaoz E, Aksoy A, Ayhan S, Sariboyaci AE, Kaymaz F, Kasap M, *et al.* Characterization of mesenchymal stem cells from rat bone marrow: Ultrastructural properties, differentiation potential and immunophenotypic markers. *Histochem Cell Biol* 2009;132:533-46.
- Lorenzi B, Pessina F, Lorenzoni P, Urbani S, Vernillo R, Sgaragli G, *et al.* Treatment of experimental injury of anal sphincters with primary surgical repair and injection of bone marrow-derived mesenchymal stem cells. *Dis Colon Rectum* 2008;51:411-20.
- Peng L, Jia Z, Yin X, Zhang X, Liu Y, Chen P, *et al.* Comparative analysis of mesenchymal stem cells from bone marrow, cartilage, and adipose tissue. *Stem Cells Dev* 2008;17:761-73.
- Liu M, Liu N, Zang R, Li Y, Yang ST. Engineering stem cell niches in bioreactors. *World J Stem Cells* 2013;5:124-35.
- Bhartiya D, Boheler K, Rameshwar P. Multipotent to pluripotent properties of adult stem cells. *Stem cell Int* 2013;2013:2.
- Furth ME, Atala A. Stem cell sources to treat diabetes. *J Cell Biochem* 2009;106:507-11.
- Tsuji O, Miura K, Okada Y, Fujiyoshi K, Mukaino M, Nagoshi N, *et al.* Therapeutic potential of appropriately evaluated safe-induced pluripotent stem cells for spinal cord injury. *Proc Natl Acad Sci U S A* 2010;107:12704-9.
- Rameshwar P. Microenvironment at tissue injury, a key focus for efficient stem cell therapy: A discussion of mesenchymal stem cells. *World J Stem Cells* 2009;1:3-7.
- Chamberlain JR, Schwarze U, Wang PR, Hirata RK, Hankenson KD, Pace JM, *et al.* Gene targeting in stem cells from individuals with osteogenesis imperfecta. *Science* 2004;303:1198-201.
- Li WJ, Tuli R, Okafor C, Derfoul A, Danielson KG, Hall DJ, *et al.* A three-dimensional nanofibrous scaffold for cartilage tissue engineering using human mesenchymal stem cells. *Biomaterials* 2005;26:599-609.
- Pasquinelli G, Tazzari P, Ricci F, Vaselli C, Buzzi M, Conte R, *et al.* Ultrastructural characteristics of human mesenchymal stromal (stem) cells derived from bone marrow and term placenta. *Ultrastruct Pathol* 2007;31:23-31.
- Abe H, Otoi T, Tachikawa S, Yamashita S, Satoh T, Hoshi H, *et al.* Fine structure of bovine morulae and blastocysts *in vivo* and *in vitro*. *Anat Embryol (Berl)* 1999;199:519-27.
- Kumar S, Ciraolo G, Hinge A, Filippi MD. An efficient and reproducible process for transmission electron microscopy (TEM) of rare cell populations. *J Immunol Methods* 2014;404:87-90.
- Baharvand H, Matthaei KI. The ultrastructure of mouse embryonic stem cells. *Reprod Biomed Online* 2003;7:330-5.
- Sathananthan H, Pera M, Trounson A. The fine structure of human embryonic stem cells. *Reprod Biomed Online* 2002;4:56-61.
- Thomson JA, Marshall VS. Primate embryonic stem cells. *Curr Top Dev Biol* 1998;38:133-65.
- Talbot NC, Garrett WM. Ultrastructure of the embryonic stem cells of the 8-day pig blastocyst before and after *in vitro* manipulation: Development of junctional apparatus and the lethal effects of PBS mediated cell-cell dissociation. *Anat Rec* 2001;264:101-13.
- Desbaillets I, Ziegler U, Groscurth P, Gassmann M. Embryoid bodies: An *in vitro* model of mouse embryogenesis. *Exp Physiol* 2000;85:645-51.
- Banfi A, Muraglia A, Dozin B, Mastrogiacomo M, Cancedda R, Quarto R, *et al.* Proliferation kinetics and differentiation potential of *ex vivo* expanded human bone marrow stromal cells: Implications for their use in cell therapy. *Exp Hematol* 2000;28:707-15.
- Chen J, Sotome S, Wang J, Orii H, Uemura T, Shinomiya K. Correlation of *in vivo* bone formation capability and *in vitro* differentiation of human bone marrow stromal cells. *J Med Dent Sci* 2005;52:27-34.
- Kretlow JD, Jin YQ, Liu W, Zhang WJ, Hong TH, Zhou G, *et al.* Donor age and cell passage affects differentiation potential of murine bone marrow-derived stem cells. *BMC Cell Biol* 2008;9:60.
- Li Y, Zhang C, Xiong F, Yu MJ, Peng FL, Shang YC, *et al.* Comparative study of mesenchymal stem cells from C57BL/10 and mdx mice. *BMC Cell Biol* 2008;9:24.
- Park SH, Park SH, Kook MC, Kim EY, Park S, Lim JH, *et al.* Ultrastructure of human embryonic stem cells and spontaneous and retinoic acid-induced differentiating cells. *Ultrastruct Pathol* 2004;28:229-38.
- Hoffding MK, Hyttel P. Ultrastructural visualization of the mesenchymal-to-epithelial transition during reprogramming of human fibroblasts to induced pluripotent stem cells. *Stem Cell Res* 2015;14:39-53.
- Csaki C, Matis U, Mobasher A, Ye H, Shakibaei M. Chondrogenesis, osteogenesis and adipogenesis of canine mesenchymal stem cells: A biochemical, morphological and ultrastructural study. *Histochem Cell Biol* 2007;128:507-20.
- Ballini A, De Frenza G, Cantore S, Papa F, Grano M, Mastrangelo F, *et al.* Ultrastructural observations of preimplantation stages of the

- sheep. *J Embryol Exp Morphol* 1976;36:609-22.
34. Ducibella T, Ukena T, Karnovsky M, Anderson E. Changes in cell surface and cortical cytoplasmic organization during early embryogenesis in the preimplantation mouse embryo. *J Cell Biol* 1977;74:153-67.
  35. Mohr LR, Trounson AO. Comparative ultrastructure of hatched human, mouse and bovine blastocysts. *J Reprod Fertil* 1982;66:499-504.
  36. Maro B, Johnson MH, Pickering SJ, Louvard D. Changes in the distribution of membranous organelles during mouse early development. *J Embryol Exp Morphol* 1985;90:287-309.
  37. Singh H, Mok P, Balakrishnan T, Rahmat SN, Zweigerdt R. Up-scaling single cell-inoculated suspension culture of human embryonic stem cells. *Stem Cell Res* 2010;4:165-79.
  38. Shalgi R, Sherman MI. Scanning electron microscopy of the surface of normal and implantation-delayed mouse blastocysts during development *in vitro*. *J Exp Zool* 1979;210:69-80.
  39. Cech S, Sedláčková M. Ultrastructure and morphometric analysis of preimplantation mouse embryos. *Cell Tissue Res* 1983;230:661-70.
  40. Hurst PR, Jefferies K, Eckstein P, Wheeler AG. An ultrastructural study of preimplantation uterine embryos of the rhesus monkey. *J Anat* 1978;126:209-20.
  41. Calarco PG, McLaren A. Ultrastructural observations of preimplantation stages of the sheep. *J Embryol Exp Morphol* 1976;36:609-22.
  42. Panigel M, Kraemer DC, Kalter SS, Smith GC, Heberling RL. Ultrastructure of cleavage stages and preimplantation embryos of the baboon. *Anat Embryol (Berl)* 1975;147:45-62.
  43. Gualtieri R, Santella L, Dale B. Tight junctions and cavitation in the human pre-embryo. *Mol Reprod Dev* 1992;32:81-7.
  44. Sathananthan H, Bongso A, Ng SC, Ho J, Mok H, Ratnam S, *et al.* Ultrastructure of preimplantation human embryos co-cultured with human ampullary cells. *Hum Reprod* 1990;5:309-18.
  45. Van Blerkom J, Manes C, Daniel JC Jr. Development of preimplantation rabbit embryos *in vivo* and *in vitro*. I. An ultrastructural comparison. *Dev Biol* 1973;35:262-82.
  46. Mohr LR, Trounson AO. Structural changes associated with freezing of bovine embryos. *Biol Reprod* 1981;25:1009-25.
  47. Plante L, King WA. Light and electron microscopic analysis of bovine embryos derived by *in vitro* and *in vivo* fertilization. *J Assist Reprod Genet* 1994;11:515-29.